Effect of notch orientation on the evolution of plasticity in superalloy single crystals

F. Ebrahimi [a,*], L.E. Forero [a], S. Siddiqui [b], N. Arakere [b]

[a] *Materials Science and Engineering Department, P.O. Box 116400, University of Florida, Gainesville, FL 32611, United States*
[b] *Mechanical and Aerospace Engineering, University of Florida, Gainesville, FL, United States*

Abstract

The effect of notch orientation on the evolution of slip bands in double-notched tensile samples of a single crystal superalloy loaded in a $\langle 0\,0\,1 \rangle$ orientation was experimentally investigated and compared to the results of a three-dimensional linear elastic anisotropic finite element analysis (FEA). The analysis was conducted for two orientations with notches parallel to a $\langle 0\,1\,0 \rangle$ and a $\langle 1\,1\,0 \rangle$ orientation, respectively. The observed slip traces agreed well with the predicted dominant slip systems based on the FEA. The experimental results suggest that the dominant slip planes activated at low load levels persist at higher load levels and the activation of other slip bands within a domain is initially inhibited.
© 2006 Elsevier B.V. All rights reserved.

Keywords: FEA; Single crystal; Superalloys; Notched samples; Slip bands; Anisotropy

1. Introduction

Single crystals of Ni-base superalloys are being used as turbine engine blades for power generation as well as in aircraft applications. In addition to creep and oxidation resistance, the blade life depends on fatigue properties. Resistance to fatigue crack initiation and propagation in metallic alloys is directly related to the development of plastic zones at notches and crack tips. Therefore, an understanding of slip activation under triaxial stress states is important in developing fatigue resistant single crystals [1,2]. Furthermore, this knowledge is also essential to the modeling of crack tip plasticity in polycrystalline materials in general.

The yielding of single crystals is usually evaluated by Schmid's law, which states that plasticity in single crystals takes place when the shear stress resolved on a slip plane and in a slip direction reaches a critical value (critical resolved shear stress (CRSS)) that is independent of the loading direction. The stress state in the vicinity of discontinuities such as notches is triaxial, and therefore, for a given loading orientation, the activated slip systems are different than those expected in tensile testing of smooth samples. Furthermore, the shape and the size of

the plastic zone are expected to depend on the crystallographic orientation of the notch.

Most experimental studies [3–5] on the stresses and strains in the vicinity of notch tips in single crystals are extensions of the original work by Rice and co-workers [6–10], which are based on the two-dimensional (2D) assumption. Recent results indicate considerable disagreement between experimental observations of the slip bands and the theoretical predictions. Crone et al. [11–13] have attempted to resolve these disagreements by incorporating anisotropic elastic as well as anisotropic hardening behaviors. However, satisfactory matching of the experimentally observed activated slip traces with the theoretically calculated slip systems has not been achieved. Perhaps the main shortcoming of the 2D plastic models is their inability to accommodate displacements along the Burgers vectors that do not lie in the plane of analysis. Recently, Flouriot et al. have conducted three-dimensional FEA of mode I crack tip in compact tension specimens for elastic ideally-plastic face-centered cubic single crystals for two orientations and have compared geometry of the crack tip strain field with the experimental observations of slip localization in cyclically loaded superalloy single crystals with similar orientations [2]. They found a good agreement between theory and experiment for one of the two orientations tested.

In this study we have used a three-dimensional (3D) finite element model that incorporates elastic anisotropy to predict

* Corresponding author. Tel.: +1 352 846 3791; fax: +1 352 846 3355.
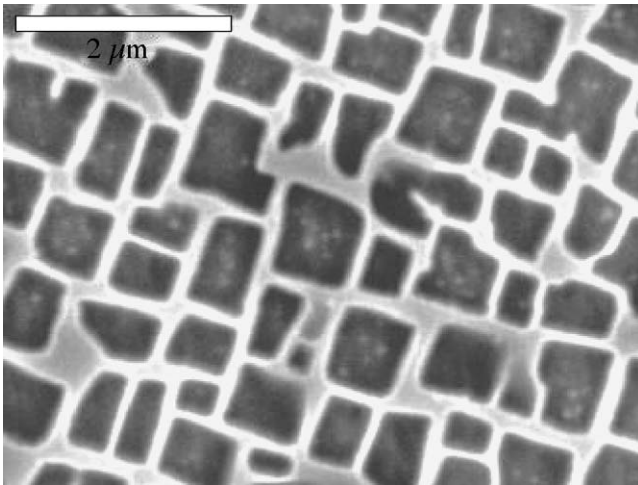 *E-mail address:* febra@mse.ufl.edu (F. Ebrahimi).

Fig. 1. SEM picture showing the tested superalloy microstructure consisting of the γ′-precipitates (dark) and γ-channels (light).

Fig. 2. Tensile engineering stress–strain curve for a sample loaded along the [0 0 1] orientation. Note that the elastic portion of the stress–strain curve does not reflect the true elastic modulus because strain values were calculated from the cross-head speed.

the slip systems activated in notched single crystals of a Ni-base superalloy loaded along a ⟨0 0 1⟩ orientation for two different notch orientations. The experiments were conducted at room temperature to ensure the activation of the {1 1 1} slip planes in both the γ-matrix and the γ′-phase. The superalloy was selected such that plastic deformation proceeded by shearing of the second phase γ′-particles. The FE analysis was conducted on specific samples for which experimental observations of the evolution of plasticity at the notch tip was conducted.

2. Material and experimental procedures

Single crystal of a Ni-base superalloy was provided in as-heat-treated condition by Pratt and Whitney. The microstructure of the alloy, which consists of cubical primary γ′-precipitates in a matrix of solid solution γ with no noticeable eutectic pool or porosity is shown in Fig. 1.

The orientations of the single crystal were determined by the Laue X-ray back-reflection technique. Dog-bone shaped tensile specimens with tensile axis approximately parallel to a ⟨0 0 1⟩ direction were cut using wire electric discharge machine (EDM). These samples had rectangular cross-sections. The crystallographic orientations of the face and the side of the samples
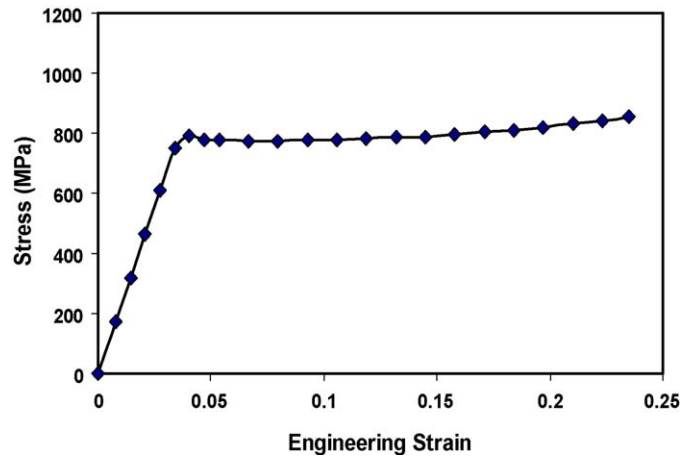
were checked after they were cut. X-ray results indicated that all expected orientations were off by no more than 8°. The average yield strength of the alloy as measured by tensile testing of un-notched samples was 794 MPa, resulting in CRSS of 324 MPa for octahedral slip systems. Fig. 2 presents the tensile stress–strain curve for a sample loaded along the [0 0 1] orientation. The yielding was distinct and the strain hardening rate was relatively small. Fig. 3 shows the slip bands at two strain levels, one immediately after the yield point and the other after fracture. The deformation began by the formation of a Lüders band (Fig. 3a), which eventually traversed the length of the sample. Fig. 3b demonstrates that the trace of other slip systems were detected at higher strain levels, which were consistent with deformation on the {1 1 1}⟨1 1 0⟩ slip systems. For a ⟨0 0 1⟩ loading orientation, multiple slip activation (8 slip systems) are expected based on the Schmid's law. The observation of the Lüders band, which is consistent with the lack of strain hardening, suggests that localization occurs easily in the superalloy investigated. Detailed analysis of tensile specimens revealed that the slip bands propagated by shearing of the γ′-precipitates. Therefore, the deformation localization can be attributed to the softening due to the particle shearing mechanism.
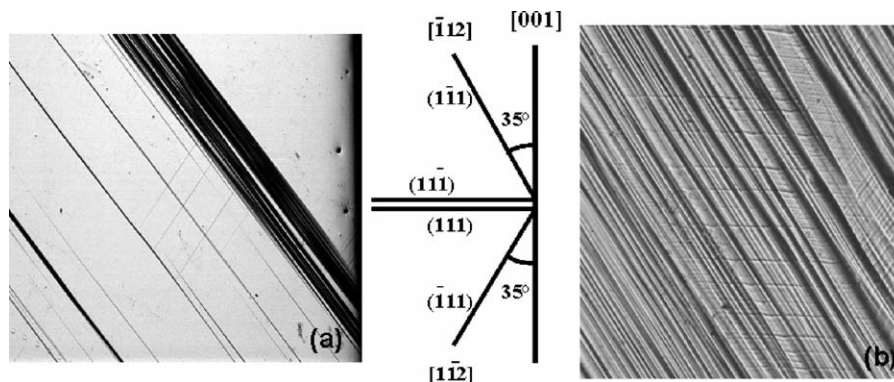

Fig. 3. Optical pictures showing the evolution of slip bands in tensile specimen (a) immediately after yielding and (b) after fracture. The middle drawing shows the trace of the different {1 1 1} slip planes on the plane of observation ((1 0 0) plane).
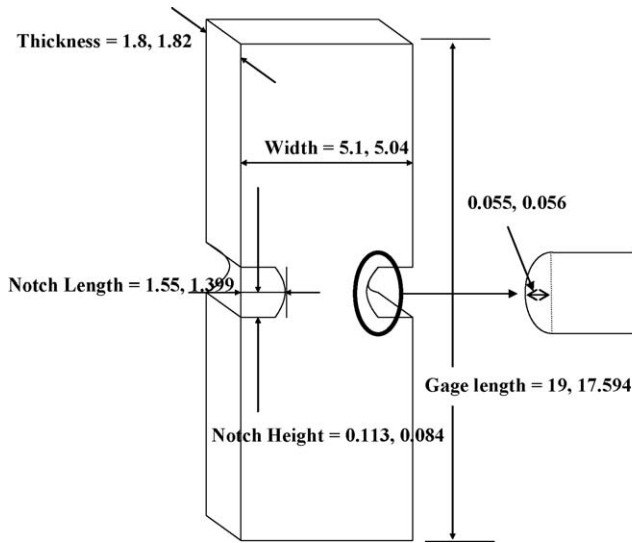
Fig. 4. Schematic of the double-notch tensile specimen used in this study. The dimensions given are representative of those used in the FEA and are in mm. For each dimension the two numbers refer to the samples with orientations A and B, respectively.

A slow speed saw with a thin diamond blade was used to cut the notches. Special fixture was designed to achieve co-planar notches with approximately equal lengths on both sides. We were able to produce consistent notch tips with careful and methodical procedures. Fig. 4 presents the dimensions of the samples. Two sample orientations with notches parallel to the [$\bar{1}$ 1 0]/[1 $\bar{1}$ 0] (orientation A) and the [0 1 0]/[0 $\bar{1}$ 0] (orientation B) directions were prepared. For both orientations, the samples were loaded along the [0 0 1] direction. Both faces of each sample were mechanically polished to remove the EDM damaged-layer and then electropolished as the final step. Samples were loaded to various levels of apparent stress intensity factors (i.e. calculated based on the sharp crack assumption [14]) in the range of $K_I = 20$–55 MPa m$^{1/2}$. The evolution of slip traces near the notches was recorded using optical microscopy.

2.1. Finite element analysis

The commercial software ANSYS (Finite Element Software Version 8.1) was employed to model the specific geometries and orientations of the double-notched tensile test specimens. The three-dimensional elements available in the ANSYS were used to justify the anisotropic linear elastic material properties. The details of the elements and the mesh used are given elsewhere [15]. The notch was modeled as an ellipse as shown schematically in Fig. 5. This geometry was very close to the shape of the notch produced by the cutting process. Since the length of the notches in each sample was not exactly the same on both sides, for the FEA model both notch lengths and heights were set equal to those of the largest actual dimensions.

The FEA component stresses around the notch were taken from the material coordinate system, i.e. the ⟨1 0 0⟩ directions, and then used in the transformation equations to calculate the individual resolved shear stresses. Table 1 presents the slip system designation used for the FE analysis as well
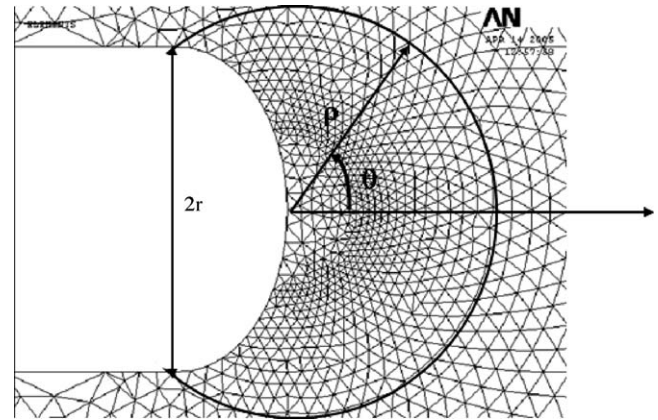

Fig. 5. Close view of the FE mesh at the notch and the definition of parameters r, ρ and θ.

as the trace of the slip planes on the (1 1 0) and (1 0 0) planes, which are the face planes of the orientations A and B, respectively. Both the γ-matrix and the γ′-precipitates have a cubic crystal structure, and therefore the elastic anisotropy of the superalloy was modeled as orthotropic with E (Young's modulus) $= 1.21 \times 10^{11}$ Pa, G (shear modulus) $= 1.29 \times 10^{11}$ Pa, and ν (Poisson's ratio) $= 0.395$ [16]. In order to evaluate the effect of incorporating elastic anisotropy, calculations were also conducted for isotropic case with $E = 2.391 \times 10^{11}$ Pa and $G = 8.354 \times 10^{10}$ Pa, estimated based on the Hashmin and Shtrikman's method [17,18]. The analysis presented in this paper is limited to the surface of the samples, since the experimental observations were made on the surface. The stress analysis results through the thickness of the samples will be presented elsewhere.

As shown in Fig. 5, the mesh design was such that resolved shear stress value, τ, for each of the 12 slip systems could be calculated at a distance ρ and angle θ with the (0,0) position at the tip of the notch. For each ρ distance, τ values were plotted as a function of θ for a given applied load level, an example of which is shown in Fig. 6 for $\rho = 5r$. In this plot, the horizontal line represents the critical resolved shear stress. At this load level, any system with a τ above the CRSS is expected to be

Table 1
Slip system designation used for the FEM analysis and the slip trace directions on the (1 1 0) and (1 0 0) planes, which are the face planes of the samples with orientations A and B, respectively

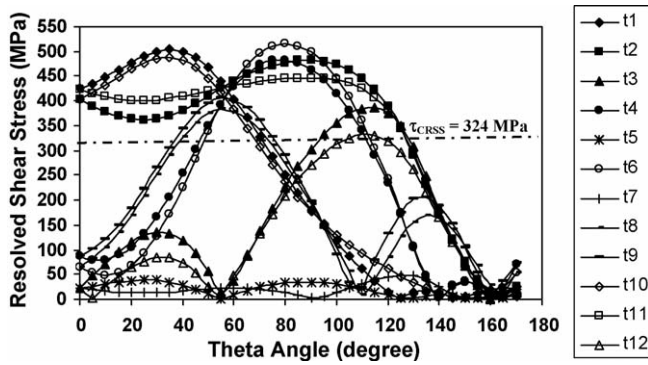| Designation	Plane	Direction	(1 1 0) Trace	(1 0 0) Trace
τ_1	(1 1 1)	[1 0 $\bar{1}$]	[1 $\bar{1}$ 0]	[0 $\bar{1}$ 1]
τ_2	(1 1 1)	[0 $\bar{1}$ 1]	[1 $\bar{1}$ 0]	[0 $\bar{1}$ 1]
τ_3	(1 1 1)	[1 $\bar{1}$ 0]	[1 $\bar{1}$ 0]	[0 $\bar{1}$ 1]
τ_4	($\bar{1}$ 1 $\bar{1}$)	[1 0 $\bar{1}$]	[$\bar{1}$ 1 2]	[0 1 1]
τ_5	($\bar{1}$ 1 $\bar{1}$)	[1 1 0]	[$\bar{1}$ 1 2]	[0 1 1]
τ_6	($\bar{1}$ 1 $\bar{1}$)	[0 1 1]	[$\bar{1}$ 1 2]	[0 1 1]
τ_7	(1 $\bar{1}$ $\bar{1}$)	[1 1 0]	[1 $\bar{1}$ 2]	[0 $\bar{1}$ 1]
τ_8	(1 $\bar{1}$ $\bar{1}$)	[0 $\bar{1}$ 1]	[1 $\bar{1}$ 2]	[0 $\bar{1}$ 1]
τ_9	(1 $\bar{1}$ $\bar{1}$)	[1 0 1]	[1 $\bar{1}$ 2]	[0 $\bar{1}$ 1]
τ_{10}	($\bar{1}$ $\bar{1}$ 1)	[0 1 1]	[1 $\bar{1}$ 0]	[0 1 1]
τ_{11}	($\bar{1}$ $\bar{1}$ 1)	[1 0 1]	[1 $\bar{1}$ 0]	[0 1 1]
τ_{12}	($\bar{1}$ $\bar{1}$ 1)	[1 $\bar{1}$ 0]	[1 $\bar{1}$ 0]	[0 1 1]

Fig. 6. Resolved shear stress values at $\rho = 5r$ for specimen with orientation A loaded to 1120 lb (4982 N).

activated. However, considering the elastic nature of the calculation, the slip system with the highest τ value will be activated first. Following this procedure, domains in which a slip system is dominant, i.e. experiences the highest resolved shear stress, can be recognized. Tables 2 and 3 present the dominant slip systems at various ρ values for orientations A and B, respectively.

3. Results and discussion

Fig. 7 presents the slip traces observed at the notch tips for orientation B loaded to various levels. The observed slip traces are symmetrical and lie along the $[0\,1\,1]$ and $[0\,1\,\bar{1}]$ directions corresponding to the activation of $(1\,1\,\bar{1})$ or $(1\,\bar{1}\,1)$ and $(1\,1\,1)$ or $(\bar{1}\,1\,1)$ slip planes, respectively. The results suggest that initially one set of planes were activated (Fig. 7a) and with increasing load the second set became activated at larger distances from the tip (Fig. 7b and c). A comparison of the FEA results with observed slip traces at two load levels for orientations B is shown in Fig. 8. The FEA results identify various domains, where in each one slip system is dominated. Because of the crystallographic symmetry of the notch only domains for 180° are presented. It should be noted that two slip systems (e.g. τ_1 or τ_{11}) are mentioned in each domain—the first represents the dominant system for the

Table 2

Numerical prediction of dominant slip systems on the surface of the orientation A, for varying radii, ρ, from the notch at applied load of 1120 lb ($K_I = 50\,\text{MPa}\,\text{m}^{1/2}$)

$r = 1\rho$		$r = 2\rho$		$r = 3\rho$		$r = 4\rho$	
θ	τ_{max}	θ	τ_{max}	θ	τ_{max}	θ	τ_{max}
0–40	τ_1	0–60	τ_1	0–60	τ_1	0–58	τ_1
40–110	τ_2	60–108	τ_2	60–68	τ_2	58–63	τ_2
–	–	108–130	τ_3	68–90	τ_6	63–94	τ_6
–	–	130–137	τ_9	90–113	τ_2	94–120	τ_2
–	–	–	–	113–138	τ_3	120–135	τ_3

$r = 5\rho$		$r = 6\rho$		$r = 7\rho$		$r = 8\rho$	
θ	τ_{max}	θ	τ_{max}	θ	τ_{max}	θ	τ_{max}
0–56	τ_1	0–55	τ_1	0–52	τ_1	0–49	τ_1
56–60	τ_2	55–59	τ_2	52–58	τ_2	49–56	τ_2
60–95	τ_6	59–95	τ_6	58–98	τ_6	56–100	τ_6
95–125	τ_2	95–124	τ_2	98–121	τ_2	100–117	τ_2
125–127	τ_3	–	–	–	–	–	–

Table 3

Numerical prediction of dominant slip systems on the surface of the orientation B, for varying radii, ρ, from the notch at applied load of 770 lb ($K_I = 45\,\text{MPa}\,\text{m}^{1/2}$)

$r = 1\rho$		$r = 2\rho$		$r = 3\rho$		$r = 4\rho$	
θ	τ_{max}	θ	τ_{max}	θ	τ_{max}	θ	τ_{max}
0–50	τ_4	0–50	τ_4	5–50	τ_4	16–48	τ_4
50–110	τ_1	50–60	τ_{11}	50–58	τ_{11}	48–57	τ_{11}
–	–	60–65	τ_{10}	58–66	τ_{10}	57–65	τ_{10}
–	–	65–132	τ_1	66–132	τ_1	65–127	τ_1

$r = 5\rho$		$r = 6\rho$		$r = 7\rho$		$r = 8\rho$	
θ	τ_{max}	θ	τ_{max}	θ	τ_{max}	θ	τ_{max}
24–46	τ_4	30–45	τ_4	85–102	τ_9	–	–
46–55	τ_{11}	45–50	τ_{11}	–	–	–	–
55–58	–	50–68	–	–	–	–	–
58–63	τ_{10}	68–85	τ_{11}	–	–	–	–
63–121	τ_1	85–110	τ_4	–	–	–	–
–	–	110–113	τ_{11}	–	–	–	–

bottom half, which corresponds to the optical picture, and the second corresponds to the top half. As it can be seen, there is an excellent agreement between the observed slip traces and those predicted by the FE calculations at both load levels.

The results for the orientation A at a relatively large load is presented in Fig. 9. There is an apparent consistency between the observed slip bands and the trace of the dominant slip systems predicted by the FEA. For detailed analysis, the position of $\rho = 5r$ is drawn on the optical picture given in Fig. 9 in order to make a comparison with the results shown in Fig. 6 and Table 2. A comparison with Table 2 reveals that the slip bands parallel to the $[\bar{1}\,1\,0]$ direction corresponding to the τ_1 and τ_2 traces extend to $\theta = 70°$, which is beyond the predicted domain boundary at 60°. According to Table 2, the numerical analysis predicts that τ_6 system is dominant between 60 and 95°, however, Fig. 9 indicates that the $[\bar{1}\,1\,2]$ trace extends from 70 to 108°, which is approximately 10° off from the expected domain boundaries. Slip bands along the $[\bar{1}\,1\,0]$ direction, which is also parallel to the τ_2 and τ_3 traces, are observed from 90 to 117° correlating with the theoretical predication of the dominance of these systems in the 95–127°.

The above evaluation confirms that within approximately 10°, the numerical analysis predicts the development of the slip bands at the notch tip for different notch orientations. It should be noted that slight crystallographic deviations of the samples as well as any loading misalignment are expected to contribute to the deviations between the experimental and numerical results. Furthermore, the rotation of the crystal during plastic deformation can also modify the angles observed.

The comparison between the experimental observations and the FEA results suggests that only the dominant slip systems (i.e. the systems with the highest resolved shear stress) and not all the slip systems with a resolved shear stress above the CRSS are activated at a given load level. For example, in Fig. 6, there are other slip systems that experience stresses above the CRSS but slip bands corresponding to their traces were not observed. As can be seen in Fig. 9, there is a region where both τ_2 and τ_6 systems are activated, which at first glance seems to be contradictory
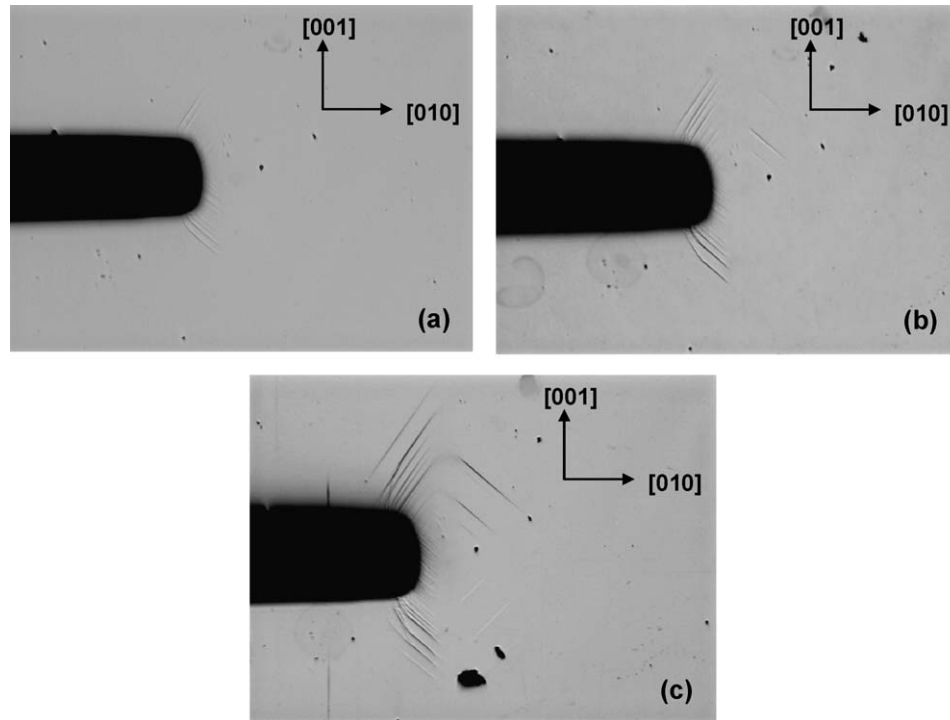
Fig. 7. Optical pictures demonstrating the evolution of the slip bands for orientation B as a function of load. (a) 432 lb ($K_I = 25$ MPa m$^{1/2}$), (b) 604 lb ($K_I = 35$ MPa m$^{1/2}$) and (c) 777 lb ($K_I = 45$ MPa m$^{1/2}$).

with the concept of the activation of only the dominant systems. This observation can be explained by the evolution of the slip as a function of load. Let us consider the order of the evolution of the slip traces at distance $\rho = 5r$ as the sample with orientation A is loaded. Because of the elastic nature of the calculation, the shape of the stress distribution curves given in Fig. 6 is independent of the load level. As the load is increased, first τ_6 and τ_1 systems are activated. At larger loads τ_2 and τ_3 systems become operational in regions outside the τ_6 and τ_1 domains. However, as the load is increased, the initial dominant slip systems, i.e. τ_6 and τ_1, persist in regions where they are not dominant but they experience a resolved shear stress above the CRSS. This persistence results in the observation of domains with more than one set of slip bands. Therefore, the overlap of the τ_2 and τ_6 domains in the 90–108° section at $\rho = 5r$ (see Fig. 9) can be attributed to the extension of the τ_6 system beyond its dominance. Two factors can contribute to the persistence of the dominant slip systems. In single-phase fcc metals the increase in the CRSS due to dislocation activity on the dominant slip system, i.e. latent hardening, makes it more difficult to activate a second slip plane within the same domain. Consequently, as the load is increased, the propagation of slip on the dominant slip systems to larger domains occurs easier than initiation of slip on new slip systems. In two-phase materials such as Ni-base superalloys, softening due to the shearing of the γ'-precipitates on the dominant slip system can further enhance the persistence of the slip on the initially deformed slip bands. As was demonstrated in Fig. 3 the superalloy investigated here is prone to softening and slip localization.

It is anticipated that the change in the strain field owing to the initiation of plasticity on the dominant slip systems would modify the resolved stresses on the non-activated slip systems. Indeed at large load levels, as shown in Fig. 10a, activation of multiple slip systems becomes prevalent. Furthermore, as shown in Fig. 10b, significant deviation in the path of the slip bands near the notch, where the stress levels are quite high may be observed. It has been shown that in Ni-base superalloys the macroscopic path of the deformation bands is a result of the complex interaction of dislocations in the γ-channels and γ'-precipitates [19,20]. Obviously the elastic analysis presented here is not capable of predicting such phenomena, but it is quite successful in anticipating which slip system will be activated initially. This is not surprising, since in complex elastic–plastic models also the initial yielding is governed by the development of stresses in the elastic region.

In order to investigate the effect of elastic anisotropy, FEA was conducted for an isotropic material. Figs. 11 and 12 compare the stress distribution at $\rho = 5r$ and load level of 1000 lb (4448 N) for orientations A and B, respectively. For both cases the maximum resolved shear stress is highest in the isotropic material. Furthermore, the incorporation of the anisotropy modifies the boundaries of the dominant slip systems. These results reveal that elastic anisotropy can have a noticeable effect on the dominance of the slip systems and hence the order of evolution of plasticity at the crack tips.

The results of this study can also shed light on the probability of fatigue crack initiation. As far as the effect of the secondary orientation (notch orientation) on fatigue crack initiation is concerned, two factors are anticipated to play important roles: (i) the level of resolved shear stresses on the slip planes and (ii) the level of normal stress on the slip plane that becomes activated first [21]. Fatigue cracks have been shown to be crystallographic and
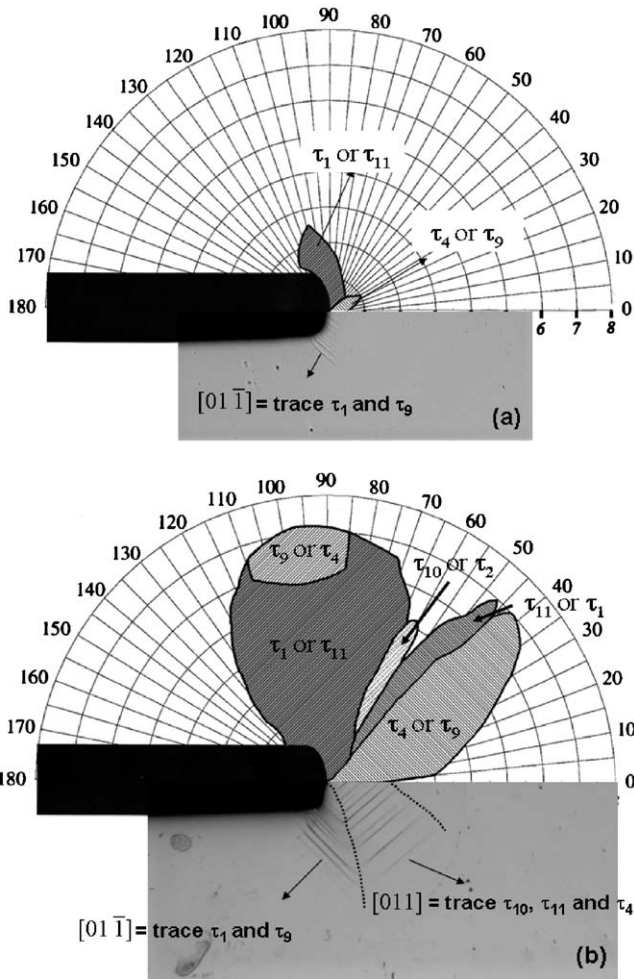
Fig. 8. Comparison of the FEA results with experimental observations for orientation B loaded to (a) $K_I = 25\,\mathrm{MPa\,m^{1/2}}$ and (b) $K_I = 45\,\mathrm{MPa\,m^{1/2}}$.
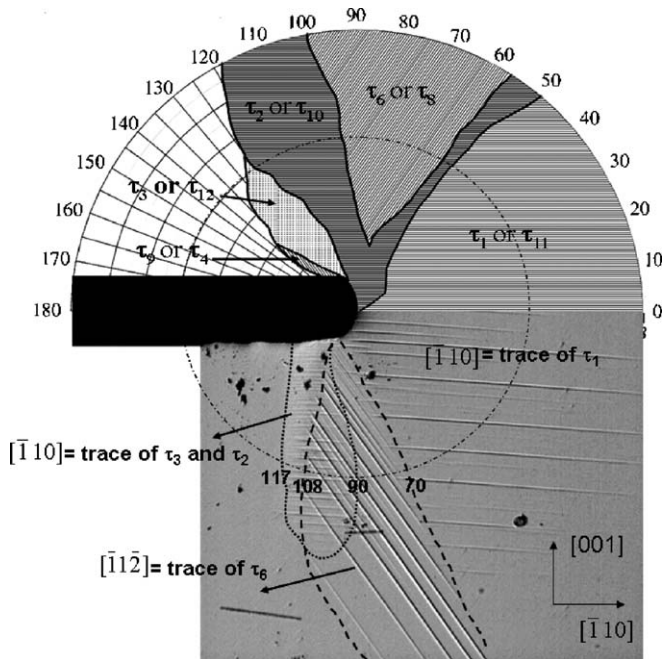

Fig. 9. Comparison of the FEA results with experimental observations for specimen with orientation A loaded to 4982 N ($K_I = 50\,\mathrm{MPa\,m^{1/2}}$).
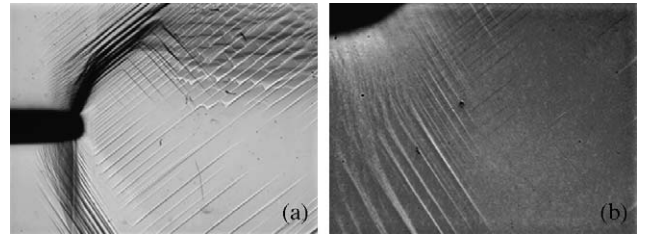

Fig. 10. Optical pictures showing (a) regions where multiple orientations of slip bands are observed and (b) extensive cross-slip near the corner of the notch in samples with B orientation at large load levels.

develop on the $\{1\,1\,1\}$ planes in single crystal Ni-base superalloys [22]. An analysis of the stresses on the notch surface, where the resolved shear stresses are the highest, predicts that plastic deformation initiates in samples with orientations A and B at applied load levels of 137.5 lb (611.6 N) and 162.7 lb (723.7 N), respectively. Based on this information it is expected that the fatigue crack initiation should take place easier for orientation A. On the other hand, the stress normal to the maximum shear stress plane at a given applied load level is higher for the orientation B than for the orientation A, e.g. at 100 lb the normal stresses are 341 and 239 MPa, respectively. When the fatigue condition is such that crack closure is important, the larger crack opening due to the presence of a higher normal stress on the crack plane may expedite the crack initiation process for the sample with orientation B.
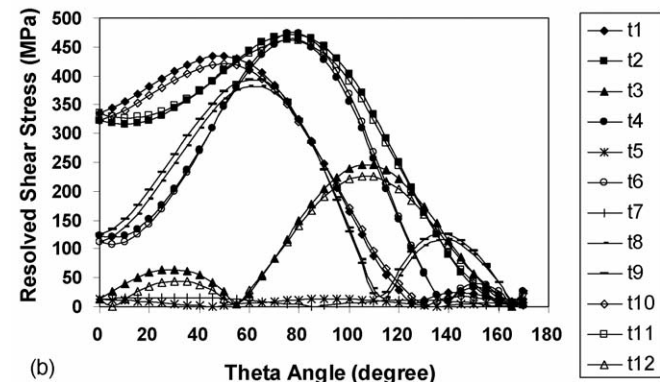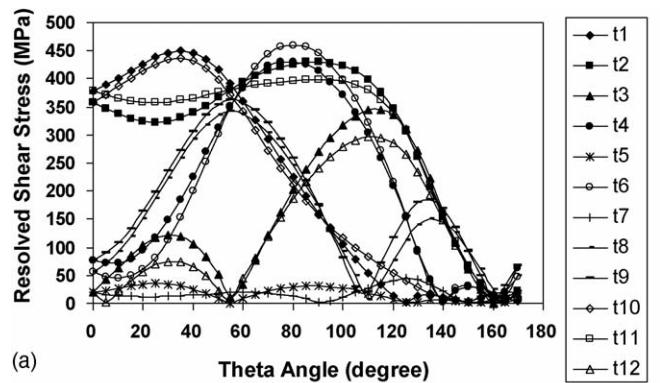

Fig. 11. Stress distribution for orientation A at distance $r = 5r$ and at load 1000 lb (4448 N). (a) Anisotropic and (b) isotropic.
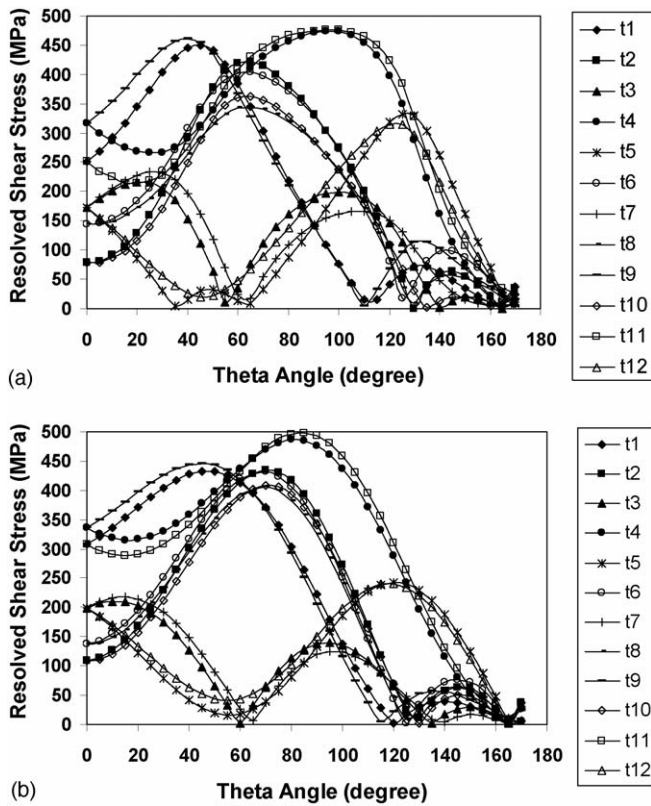
Fig. 12. Stress distribution for orientation B at distance $r = 5r$ and at load 1000 lb (4448 N). (a) Anisotropic and (b) isotropic.

4. Conclusions

The evolution of slip traces in double-notched tensile specimens of a single crystal superalloy was studied as a function of load and compared to the results of a three-dimensional anisotropic elastic finite element analysis. This comparison resulted in the following conclusions:

(1) The predictions based on the numerical analysis are in good agreement with the experimental observation of slip near notched samples and suggest that deformation is initiated on the slip systems with the highest resolved shear stress (dominant slip systems).
(2) Slip on the dominant slip systems persists as the load is increased and new slip systems do not become activated even when the stress level on them reaches the CRSS. This finding is attributed to the latent hardening and softening of the dominant slip systems due to the γ'-particle shearing.
(3) The incorporation of elastic anisotropy can have noticeable effect on the modeling of slip evolution at discontinuities.

References

[1] N. Arakere, G.J. Swanson, Eng. Mat. Gas Turbines Power 134 (2002) 161.
[2] S. Flouriot, S. Forest, G. Cailletaud, A. Koster, L. Remy, B. Burgardt, V. Gros, S. Mosset, J. Delautre, Int. J. Fract. 124 (2003) 43.
[3] T.W. Shield, Acta Mater. 44 (1996) 1547.
[4] X.M. Li, F.P. Chiang, J. Wu, M. Dudley, Eng. Fract. Mech. 43 (1992) 171.
[5] T.W. Shield, K.S. Kim, J. Mech. Phys. Solids 42 (1994) 845.
[6] J.R. Rice, Mech. Mater. 6 (1987) 317.
[7] J.R. Rice, M. Saeedvafa, J. Mech. Phys. Solids 35 (1987) 189.
[8] M. Saeedvafa, J.R. Rice, J. Mech. Phys. Solids 37 (1989) 673.
[9] J.R. Rice, D.E. Hawk, R.J. Asaro, Int. J. Fract. 42 (1990) 301.
[10] M. Saeedvafa, J.R. Rice, Modell. Simul. Mater. Sci. Eng. 1 (1992) 53.
[11] W.C. Crone, T. Shield, J. Mech. Phys. Solids 49 (2001) 2819.
[12] W.C. Crone, T. Shield, J. Mech. Phys. Solids 51 (2003) 1623.
[13] W.C. Crone, T.W. Shield, A. Creuziger, B. Henneman, J. Mech. Phys. Solids 52 (2004) 85.
[14] D. Broek, Elementary Engineering Fracture Mechanics, third ed., Martinus Nijhoff Publishers, 1984, 76.
[15] N.K. Arakere, S. Magnan, S. Siddiqui, L.E. Forero, F. Ebrahimi, ASME J. Eng. Gas Turbines Power 127 (2005) 629.
[16] S. Kalluri, A. Abdul-Aziz, M.A. McGaw, Elastic Response of [0 0 1]-Oriented PWA 1480 Single Crystal—The influence of Secondary Orientation, NASA TM-103782, 1991.
[17] Z. Hashmin, S. Shtrikman, J. Mech. Phys. Solids 10 (1962) 335.
[18] Z. Hashmin, S. Shtrikman, J. Mech. Phys. Solids 10 (1962) 343.
[19] E. Westbrooke, Effect of crystallographic orientation on plastic deformation of single crystal nickel-based superalloys, Ph.D. Dissertation, University of Florida, 2005.
[20] E. Westbrooke, L.E. Forero, F. Ebrahimi, Acta Mater. 53 (2005) 2137.
[21] R.K. Nalla, J.P. Campbell, R.O. Ritchie, Int. J. Fatigue 24 (2002) 1047.
[22] D. Deluca, C. Annis, Fatigue in Single Crystal Superalloys, Office of Naval Research, FR23800, August 1995.